Wang *et al. Microstructures* **2025**, *5*, 2025024
DOI: 10.20517/microstructures.2024.76

Microstructures

Research Article

Open Access

Check for updates

Pt quantum dots coupled with NiFe LDH nanosheets for efficient hydrogen evolution reaction at industrial current densities

Boxue Wang[1,#], Xinru Zhao[1,#], Huachuan Sun[1], Mengling Zhang[1], Mingpeng Chen[1], Guoyang Qiu[1], Tong Zhou[1], Dequan Li[1], Yuewen Wu[1], Chen Liu[1], Hang Yang[1], Qinjie Lu[1], Jianhong Zhao[1], Yumin Zhang[1], Jin Zhang[1], Hao Cui[2], Feng Liu[2], Qingju Liu[1]

[1]National Center for International Research on Photoelectric and Energy Materials, Yunnan Key Laboratory for Micro/Nano Materials & Technology, School of Materials and Energy, Yunnan University, Kunming 650091, Yunnan, China.
[2]Yunnan Precious Metals Laboratory Co., Ltd., Kunming 650106, Yunnan, China.
[#]These authors contributed equally to this work.

Correspondence to: Dr. Huachuan Sun, National Center for International Research on Photoelectric and Energy Materials, Yunnan Key Laboratory for Micro/Nano Materials & Technology, School of Materials and Energy, Yunnan University, No. 2 Cuihu North Road, Wuhua District, Kunming 650091, Yunnan, China. E-mail: huachuansun@ynu.edu.cn; Prof. Qingju Liu, National Center for International Research on Photoelectric and Energy Materials, Yunnan Key Laboratory for Micro/Nano Materials & Technology, School of Materials and Energy, Yunnan University, No. 2 Cuihu North Road, Wuhua District, Kunming 650091, Yunnan, China. E-mail: qjliu@ynu.edu.cn

How to cite this article: Wang, B.; Zhao, X.; Sun, H.; Zhang, M.; Chen, M.; Qiu, G.; Zhou, T.; Li, D.; Wu, Y.; Liu, C.; Yang, H.; Lu, Q.; Zhao, J.; Zhang, Y.; Zhang, J.; Cui, H.; Liu, F.; Liu, Q. Pt quantum dots coupled with NiFe LDH nanosheets for efficient hydrogen evolution reaction at industrial current densities. *Microstructures* **2025**, *5*, 2025024. https://dx.doi.org/10.20517/microstructures.2024.76

Received: 26 Aug 2024 **First Decision:** 25 Sept 2024 **Revised:** 16 Oct 2024 **Accepted:** 28 Oct 2024 **Published:** 26 Feb 2025

Academic Editor: Zhigang Chen **Copy Editor:** Guomiao Wang **Production Editor:** Guomiao Wang

Abstract

Developing efficient and economical electrocatalysts for hydrogen generation at high current densities is crucial for advancing energy sustainability. Herein, a self-supported hydrogen evolution reaction (HER) electrocatalyst is rationally designed and prepared on a nickel foam through a simple two-step chemical etching method, which consists of Pt quantum dots (Pt_{QDs}) coupled with nickel-iron layered double hydroxide (NiFe LDH) nanosheets (named Pt_{QDs}@NiFe LDH). The characterization results indicate that the introduction of Pt_{QDs} induces more oxygen vacancies, thereby optimizing the electronic structure of Pt_{QDs}@NiFe LDH. This modification enhances the conductivity and accelerates the adsorption/desorption kinetics of hydrogen intermediates in Pt_{QDs}@NiFe LDH, ultimately resulting in exceptional catalytic performance for the HER at large current densities. Specifically, Pt_{QDs} @NiFe LDH delivers 500 and 2000 mA·cm^{-2} with remarkably low overpotentials of 92 and 252 mV, respectively,

markedly outperforming commercial Pt/C (η_{500} = 190 mV, η_{2000} = 436 mV). Moreover, when employing NiFe LDH precursor and the prepared Pt_{QDs}@NiFe LDH catalyst as the anode and cathode, respectively, in an overall water electrolysis system, only 1.66 V and 2.02 V are required to achieve 500 and 2000 mA·cm^{-2}, respectively, while maintaining robust stability for 200 h. This study introduces a feasible approach for developing HER electrocatalysts to achieve industrial-scale current densities.

Keywords: Pt quantum dots, electronic structure regulation, NiFe layered double hydroxide, industrial-level current density, hydrogen evolution reaction

INTRODUCTION

The primary source of energy consumption remains to be fossil fuels[1-3]. However, the widespread consumption of fossil fuels during industrialization not only triggers an energy crisis but also leads to a series of global issues, such as extreme weather, environmental pollution, and global temperature rise[4-8]. To achieve sustainable development of human society, numerous researchers are urgently seeking zero-carbon, easily accessible green energy sources to replace traditional energy in the foreseeable future[9]. Hydrogen (H_2) has attracted considerable interest as a clean fuel owing to its impressive calorific value of 142 MJ/kg and its crucial role as an industrial raw material, including ammonia synthesis, methanol synthesis, and metal smelting[10-14]. Among the various methods for H_2 generation, electrochemical water splitting technology offers an ideal means of converting the unstable electricity provided by intermittent energy sources such as wind and tidal energy into high-purity H_2[15-17]. Unfortunately, the electrochemical water splitting involves a two-electron transfer process at the cathode (hydrogen evolution reaction, HER) and a four-electron transfer process at the anode (oxygen evolution reaction, OER), which results in significant kinetic barriers[18-20]. Therefore, it is imperative to research and develop inexpensive and efficient electrocatalysts to enhance both HER and OER.

Based on this situation, tremendous efforts have been dedicated to the research of HER electrocatalysts, resulting in major progress in recent years. Among the various materials, transition metal (TM)-based electrocatalysts, including TM-oxides, TM-hydroxides, TM-alloys, TM-nitrides, and TM-sulfides, have been extensively reported[21-26]. Among them, researchers have demonstrated significant interest in TM layered double hydroxides (TM-LDHs) owing to their exceptional two-dimensional layered structure, which endows them with distinctive electronic structures, tunable chemical compositions, and large specific surface areas[27-29]. The NiFe LDH, as one of the TM-LDH electrocatalysts, has gained widespread recognition for its extensive application potential due to its abundant raw materials, cost-effectiveness, and exceptional catalytic performance in the OER process[30,31]. However, the affinity for NiFe LDH with H is relatively weak, resulting in a poor ability to cleave the H-O-H bond, which leads to a high energy barrier for HER in alkaline media[32,33]. Furthermore, the inadequate conductivity of NiFe LDH and the restricted active sites also adversely affect its HER performance[34,35]. Therefore, it is crucial to adopt effective strategies to bolster the intrinsic activity of NiFe LDH and optimize the adsorption/desorption of H intermediates to improve the HER catalytic performance. For instance, Chen *et al.*[32] achieved successful substitution of some Fe atoms in NiFe LDH with Ru atoms (NiFeRu LDH) using a one-pot hydrothermal method to create an efficient difunctional electrocatalyst. The NiFeRu LDH electrocatalyst requires overpotentials of 29 mV (for HER) and 225 mV (for OER) to achieve 10 mA·cm^{-2} in 1 M KOH. The experimental and theoretical calculations demonstrate that the introduction of Ru atoms can lower the energy barrier, and effectively accelerate the HER reaction kinetics. Although the HER performance of non-precious metal-based electrocatalysts has been greatly improved, it still lags behind that of precious metal-based electrocatalysts[36-39]. Unfortunately, the high cost, scarcity, and poor stability of precious metals pose significant barriers to their large-scale industrial applications[40,41]. Practical experience has proven that the

electrocatalytic performance can be significantly improved and costs can be reduced by reducing the usage of precious metals, decreasing their size, and combining them with non-precious metals[42]. For example, Lei *et al.*[10] prepared Pt quantum dot (Pt_{QDs}) coupled S-doped NiFe LDH HER electrocatalysts (Pt@S-NiFe LDHs) with a Pt loading content of only 4.68% using hydrothermal and electrodeposition methods. Pt@S-NiFe LDHs exhibit excellent HER performance due to the optimized binding energy (BE), rapid mass transport, and gas release. However, there is room for improvement in enhancing its catalytic activity and stability at ampere-level current density.

In this work, we successfully dispersed Pt_{QDs} on the NiFe LDH nanosheet surface (Pt_{QDs}@NiFe LDH) using a two-step simple chemical etching method. The characterization results indicate that the strong electronic interactions between the Pt_{QDs} and NiFe LDH in Pt_{QDs}@NiFe LDH, which adjusts the electronic structure and accelerates the HER reaction kinetics, ultimately leading to excellent HER performance at high current densities (> 500 $mA{\cdot}cm^{-2}$). Specifically, the Pt_{QDs}@NiFe LDH electrocatalyst only needs the overpotentials of 53 and 140 mV to realize 100 and 1000 $mA{\cdot}cm^{-2}$, respectively. In addition, the Pt_{QDs}@NiFe LDH electrocatalyst can deliver 2000 $mA{\cdot}cm^{-2}$ with a low overpotential of 252 mV. Furthermore, a two-electrode cell was constructed with Pt_{QDs}@NiFe LDH serving as the cathode and NiFe LDH acting as the anode [Pt_{QDs}@NiFe LDH (-) || NiFe LDH (+)], achieving 100 and 1000 $mA{\cdot}cm^{-2}$ of mere potentials of 1.54 and 1.75 V, respectively. This research offers valuable insights for the advancement of affordable and efficient electrocatalysts.

MATERIALS AND METHODS

Preparation of NiFe LDH

In detail, 2.02 g of $Fe(NO_3)_3{\cdot}9H_2O$ was dissolved in 50 mL of deionized (DI) water and sonicated for 5 min to form a homogeneous solution. A clean nickel foam (NF) substrate (2 × 3 cm^2) was then immersed in the mixture and reacted at room temperature (25 ℃) for 8.5 h. Upon completion of the reaction, the sample was rinsed several times with DI water and anhydrous ethanol, and then dried in an oven at 50 ℃ for 12 h to obtain the NiFe LDH-8.5 (abbreviated as Pt_{QDs}@NiFe LDH) precursor. To obtain the optimal sample, additional samples were prepared with reaction times of 6.5 and 10.5 h, respectively, and named NiFe LDH-6.5 and NiFe LDH-10.5, respectively.

Preparation of Pt_{QDs}@NiFe LDH

The synthesis of Pt_{QDs}@NiFe LDH was also achieved through a chemical etching method. Firstly, 20 mg $H_2PtCl_6{\cdot}6H_2O$ was added to 4 mL DI water and 6 mL anhydrous ethanol, and the mixture was sonicated for 10 min to form a homogeneous solution. Secondly, the NiFe LDH (2 × 3 cm^2) was completely immersed in the mixture and reacted at room temperature (25 ℃) for 3 h. Finally, upon completion of the reaction, the sample was rinsed several times with DI water and anhydrous ethanol, and then dried in an oven at 50 ℃ for 12 h to obtain Pt_{QDs}@NiFe LDH-3 (abbreviated as Pt_{QDs}@NiFe LDH). The mass loading of Pt species on the NiFe LDH was determined to be 1.4 $mg{\cdot}cm^{-2}$ by weighing the sample before and after the reaction. To obtain the optimal sample, additional samples were prepared with reaction times of 1 and 5 h, respectively, and named Pt_{QDs}@NiFe LDH-1 and Pt_{QDs}@NiFe LDH-5, respectively. The mass loadings of Pt species of Pt_{QDs}@NiFe LDH-1 and Pt_{QDs}@NiFe LDH-5 were measured as 0.3 $mg{\cdot}cm^{-2}$ and 2.1 $mg{\cdot}cm^{-2}$, respectively.

RESULTS AND DISCUSSION

Characterization results

The self-supported Pt_{QDs}@NiFe LDH was obtained through a two-step feasible chemical etching method. As shown in Figure 1A, NF was first immersed in $Fe(NO_3)_3{\cdot}9H_2O$ solution and reacted for 8.5 h to synthesize the NiFe LDH precursor. Then, the NiFe LDH precursor was placed in $H_2PtCl_6{\cdot}6H_2O$ solution for 3 h to synthesize the Pt_{QDs}@NiFe LDH electrocatalyst. In this process, Pt^{4+} is reduced to Pt^0 due to the electrode

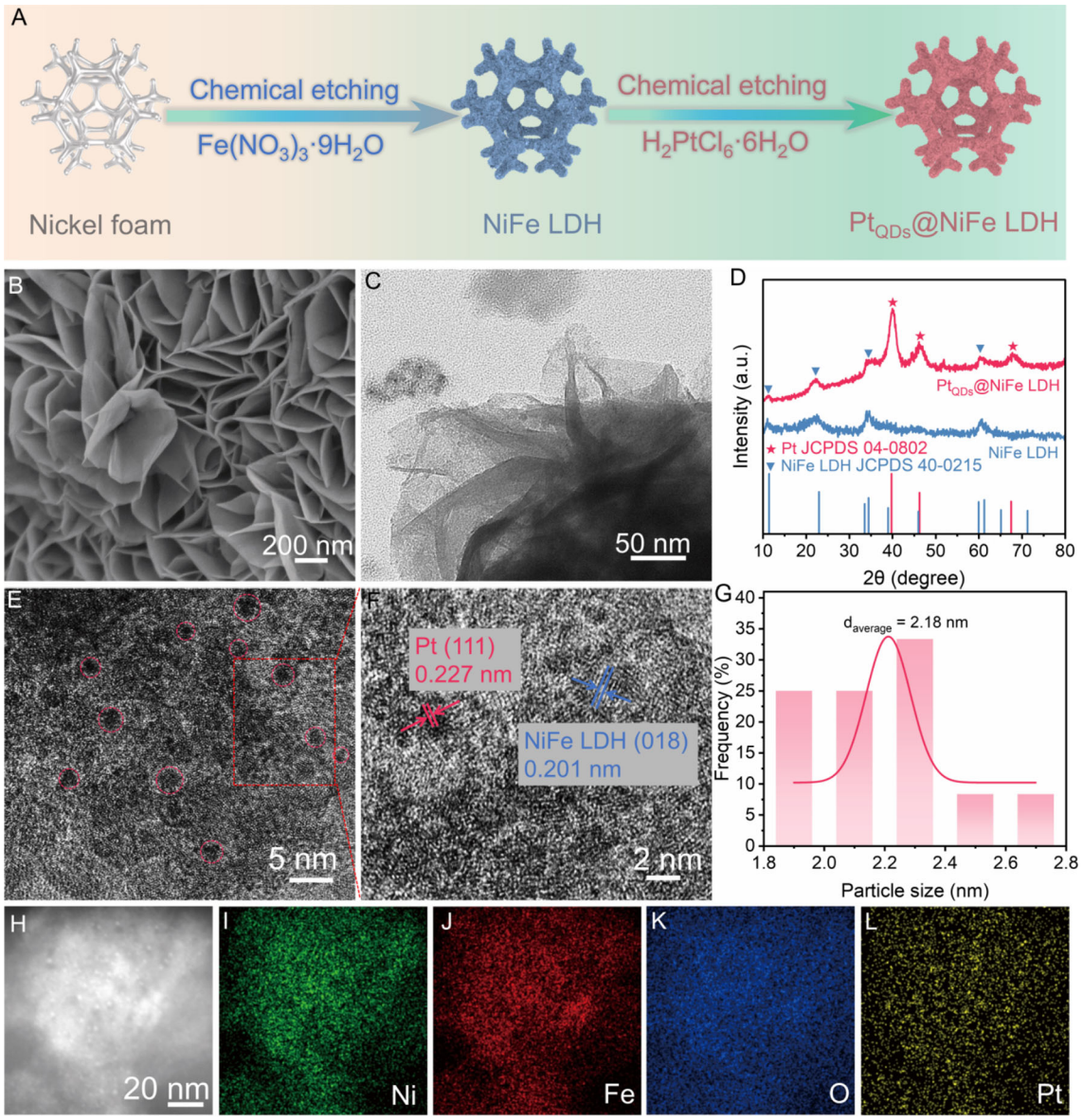

Figure 1. The structure and morphology of Pt_{QDs}@NiFe LDH. (A) The schematic synthesis route. (B, C) SEM and TEM images of Pt_{QDs} @NiFe LDH. (D) XRD patterns of Pt_{QDs}@NiFe LDH and NiFe LDH. (E, F) HRTEM images of Pt_{QDs}@NiFe LDH (the Pt_{QDs} are marked with pink circles). (G) The size distribution of Pt_{QDs}. (H-L) EDS images of Pt_{QDs}@NiFe LDH.

potential difference between $E^{o}_{Ni(II)/(0)}$(-0.257 V) and $E^{o}_{Pt(IV)/(0)}$(+1.188 V) [*vs.* standard hydrogen electrode (SHE)], along with the reductive properties of ethanol. The microstructures of the synthesized samples were investigated via scanning electron microscopy (SEM) and transmission electron microscopy (TEM). Supplementary Figure 1 shows the orderly arrangement of NiFe LDH nanosheet arrays on NF. The nanosheets with large specific surface areas offer numerous available sites for introducing Pt_{QDs}. In Figure 1B, 1C, and Supplementary Figure 2, the structure of Pt_{QDs}@NiFe LDH remains as nanosheets after chemical etching for 1, 3, and 5 h. This indicates that the incorporation of Pt_{QDs} does not destroy the architecture of NiFe LDH nanosheets. To determine the crystal structures of synthesized samples, X-ray diffraction (XRD) was performed. The characteristic peaks corresponding to NiFe LDH (PDF# 40-0215) are clearly observed, indicating that the NiFe LDH precursor is successfully synthesized [Figure 1D][43]. For Pt_{QDs}

@NiFe LDH, besides the peaks of NiFe LDH, there are peaks at 39.7°, 46.2°, and 67.4°, attributed to the (111), (200), and (220) planes of Pt (PDF# 40-0802), suggesting that Pt is likely coupled in the form of QDs on the NiFe LDH[10]. Additional examinations were carried out on NiFe LDH and Pt_{QDs}@NiFe LDH utilizing high-resolution TEM (HRTEM). Supplementary Figure 3 indicates that the interplanar spacing of 0.225 nm corresponds to the (015) plane of NiFe LDH which is consistent with the XRD result. Moreover, Figure 1E and 1F shows that the Pt_{QDs} disperse on the NiFe LDH nanosheets and marked with pink circles are observed. The interplanar spacings of 0.201 and 0.227 nm belong to the (018) plane of NiFe LDH and the (111) plane of Pt, respectively, demonstrating that Pt_{QDs} are coupled with the NiFe LDH. Additionally, statistical analysis of the Pt_{QDs} in Figure 1E, 1G and Supplementary Figure 4 uncovers that the average diameter of the Pt_{QDs} in Pt_{QDs}@NiFe LDH is approximately 2.2 nm. The energy dispersive spectroscopy (EDS) images illustrate the presence of Ni, Fe, O, and Pt elements of Pt_{QDs}@NiFe LDH, and the distribution of Pt is dispersed [Figure 1H-L]. This is advantageous for improving the HER performance of Pt_{QDs}@NiFe LDH. The mass loading of Pt species on the NiFe LDH was determined to be 1.4 mg·cm^{-2}. Furthermore, inductively coupled plasma optical emission spectrometry (ICP-OES) analysis revealed that Pt_{QDs}@NiFe LDH contains 7.08% Pt by mass, contributing significantly to the abundance of active sites for the HER process [Supplementary Table 1].

The surface electronic structure and chemical states of obtained samples were revealed through X-ray photoelectron spectroscopy (XPS). Figure 2A reveals that the Ni, Fe, and O elements are present in NiFe LDH precursor, while the Ni, Fe, O, and Pt elements are present in Pt_{QDs}@NiFe LDH. This aligns with the EDS result of Pt_{QDs}@NiFe LDH, further indicating that Pt has been successfully introduced into NiFe LDH. For NiFe LDH, the characteristic peaks located at 855.34 and 872.96 eV are assigned to $2p_{3/2}$ and $2p_{1/2}$ of Ni^{2+}, respectively, accompanied by two satellite peaks, while the peak at 852.19 eV corresponds to Ni^0 [Figure 2B][24,44-46]. The peaks at 711.24 and 724.27 eV are assigned to Fe^{3+} $2p_{3/2}$ and $2p_{1/2}$, respectively, accompanied by two satellite peaks [Figure 2C][5,43]. Compared to NiFe LDH, the BEs of Ni 2p and Fe 2p in Pt_{QDs}@NiFe LDH are shifted positively by approximately 0.33 and 0.34 eV, respectively, indicating that the coupling between Pt_{QDs} and NiFe LDH induces strong electronic interactions in Pt_{QDs}@NiFe LDH. For Pt 4f XPS spectra of Pt_{QDs}@NiFe LDH [Figure 2D], it can be observed that the peaks at 71.21 and 74.46 eV are attributed to Pt^0 $4f_{7/2}$ and $4f_{5/2}$, respectively[47]. Meanwhile, the peaks at 72.50 and 76.32 eV are assigned to Pt^{2+} $4f_{7/2}$ and $4f_{5/2}$, respectively[10,48]. This indicates that the predominant form of Pt is metallic Pt, which confirms the successful preparation of Pt_{QDs}.

In addition, Figure 2E shows that the O 1s XPS spectra of NiFe LDH are fitted into four peaks, identified as lattice oxygen (M-O, 529.51 eV), hydroxyl oxygen (M-OH, 531.01 eV), oxygen vacancies (O_v, 532.17 eV), and adsorbed H_2O (533.32 eV)[35,49]. Notably, there is a positive shift of approximately 0.27 eV in the BE of the O 1s in Pt_{QDs}@NiFe LDH compared to NiFe LDH. This serves as additional evidence that the interaction between Pt_{QDs} and NiFe LDH in Pt_{QDs}@NiFe LDH leads to strong electronic interactions, potentially optimizing the electronic structure. Moreover, the presence of O_v in Pt_{QDs}@NiFe LDH and NiFe LDH was further confirmed by electron paramagnetic resonance (EPR). Figure 2F shows a distinct signal of g = 2.003, which corresponds to O_v[50]. The intensity observed in Pt_{QDs}@NiFe LDH is significantly higher than that in comparison to NiFe LDH. This indicates the presence of a more abundant amount of O_v in Pt_{QDs}@NiFe LDH. To gain a deeper understanding of the impacts of O_v on Pt_{QDs}@NiFe LDH electrocatalyst, density functional theory (DFT) was employed. The calculated models include NiFe LDH without O_v, NiFe LDH with O_v, Pt_{QDs}@NiFe LDH without O_v, and Pt_{QDs}@NiFe LDH with O_v [Supplementary Figure 5]. The formation energies of O_v in NiFe LDH and Pt_{QDs}@NiFe LDH are calculated to be -0.024 and -0.259 eV, respectively, indicating that the formation of O_v in both NiFe LDH and Pt_{QDs}@NiFe LDH is thermodynamically spontaneous, and the introduction of Pt_{QDs} promotes the formation of O_v. This finding

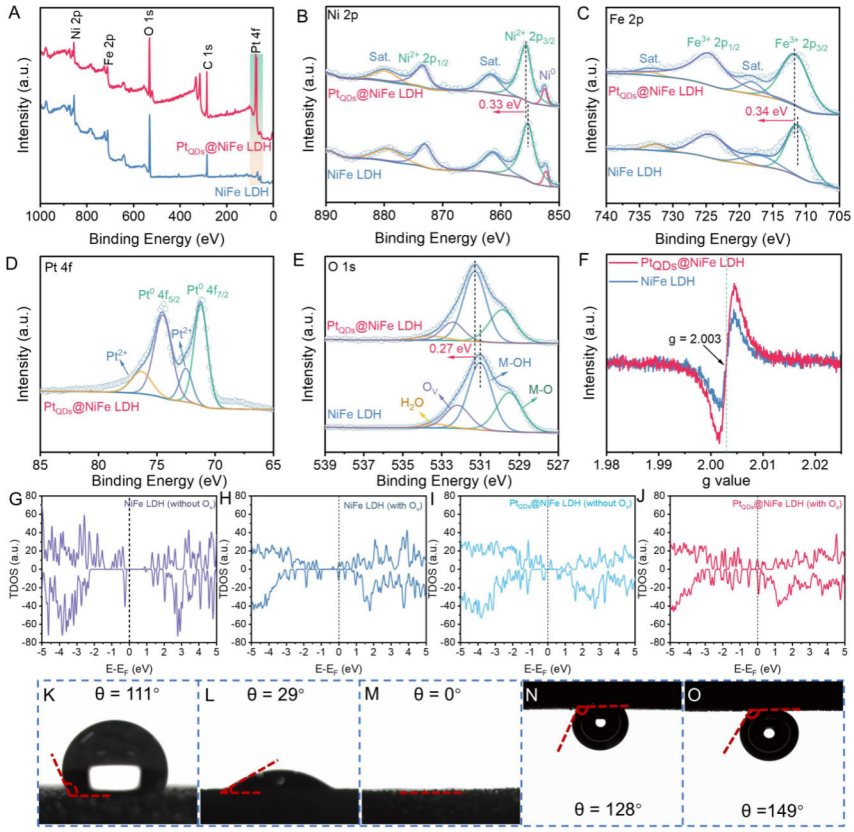

Figure 2. The surface electronic structure and contact angles of the synthesized samples. (A) XPS survey spectra. The XPS spectra of (B) Ni 2p, (C)Fe 2p, (D) Pt 4f and (E) O 1s. (F) EPR spectra. (G-H) TDOS of NiFe LDH without O_v, NiFe LDH with O_v, Pt_{QDs}@NiFe LDH without O_v and Pt_{QDs}@NiFe LDH with O_v. (K-M) The contact angles. (N, O) The bubble contact angles.

aligns with the results of XPS and EPR, reconfirming that Pt_{QDs}@NiFe LDH contains a higher concentration of O_v. The increased concentration of O_v in Pt_{QDs}@NiFe LDH serves to optimize the H adsorption/desorption process and promote water dissociation, thereby improving the kinetics of HER[51,52]. Furthermore, the electronic structure of Pt_{QDs}@NiFe LDH was analyzed by calculating the total density of states (TDOS) to assess the effects of O_v formation and Pt_{QDs} introduction. Figure 2G-J indicates that after the formation of O_v, the conduction band crosses the Fermi level (E_F), suggesting that the formation of O_v can effectively enhance conductivity. Additionally, the introduction of Pt_{QDs} significantly reduces the bandgap and increases the intensity of TDOS near E_F, indicating that the incorporation of Pt_{QDs} also enhances conductivity. These results collectively demonstrate that Pt_{QDs}@NiFe LDH possesses superior conductivity, thereby promoting efficient charge transfer and facilitating the HER[53,54]. In addition, the adsorption capability of Pt_{QDs}@NiFe LDH for H intermediates was revealed through surface valence band photoemission spectroscopy. In Supplementary Figure 6, the d-band centers of NiFe LDH and Pt_{QDs}@NiFe LDH are -5.85 eV and -5.08 eV, respectively. This not only indicates that the introduction of Pt adjusts the d-band center of Pt_{QDs}@NiFe LDH to be more proximate to the E_F, but also elucidates that Pt_{QDs}@NiFe LDH has a stronger adsorption capability for H intermediates, which is likely to be beneficial for enhancing the HER performance of Pt_{QDs}@NiFe LDH[45,55].

The surface properties of Pt_{QDs}@NiFe LDH and NF were further evaluated by measuring the contact angles and bubble contact angles of Pt_{QDs}@NiFe LDH and NF. Figure 2K and Supplementary Figure 7A show that the contact angle of NF is greater than 110° from the initial stage to 1.5 s, indicating its hydrophobic nature.

The contact angle of NiFe LDH decreases from 98° at initial stage to 29° at 1.5 s, indicating its hydrophilic nature [Figure 2L and Supplementary Figure 7B]. In contrast to NF and NiFe LDH, the contact angle of Pt_{QDs}@NiFe LDH remains 0° from the initial stage to 1.5 s, demonstrating its superhydrophilicity, which can facilitate the intimate contact between Pt_{QDs}@NiFe LDH and the solution, thereby contributing to the enhancement of HER performance [Figure 2M and Supplementary Figure 7C][56]. In addition, the bubble contact angles were also measured to assess electrocatalytic performance. Figure 2N and 2O indicates that the bubble contact angles of Pt_{QDs}@NiFe LDH and NF are 149° and 128°, respectively. This demonstrates that Pt_{QDs}@NiFe LDH exhibits superaerophobicity, which ensures the rapid detachment of H_2 bubbles from the surface of Pt_{QDs}@NiFe LDH during the HER process, thereby accelerating reaction kinetics. The superhydrophilic and superaerophobic properties of Pt_{QDs}@NiFe LDH suggest that it possesses fast mass/charge transfer, which will enhance the HER reaction kinetics[10,36].

HER performance

The HER performance of the samples was assessed in 1 M KOH solution. First, the linear sweep voltammetry (LSV) curves indicate that the HER activity of NiFe LDH is significantly superior to that of NiFe LDH-6.5 and NiFe LDH-10.5 [Supplementary Figure 8]. Supplementary Figure 9 indicates that the HER activity of Pt_{QDs}@NiFe LDH is significantly superior to that of Pt_{QDs}@NiFe LDH-1 and Pt_{QDs}@NiFe LDH-5. Moreover, Pt_{QDs}@NiFe LDH also exhibits superior HER performance compared to NiFe LDH, Pt/C, and NF [Figure 3A, B]. Specifically, Pt_{QDs}@NiFe LDH only requires 53, 140, and 252 mV of overpotentials to 100, 1000, and 2000 $mA{\cdot}cm^{-2}$, respectively, which is far lower than NiFe LDH (η_{100} = 336 mV, η_{1000} = 515 mV, and η_{2000} = 676 mV), Pt/C (η_{100} = 67 mV, η_{1000} = 280 mV, and η_{2000} = 436 mV), and NF (η_{100} = 284 mV, η_{1000} = 474 mV, and η_{2000} = 641 mV). Furthermore, the reaction kinetics of synthesized samples were further evaluated using Tafel slopes. Supplementary Figure 10 illustrates that the Tafel slope of Pt_{QDs}@NiFe LDH is 35 $mV\ dec^{-1}$, which is notably lower than other control samples. This indicates that Pt_{QDs}@NiFe LDH exhibits the most rapid reaction kinetics compared to the other samples and the rate-determining step in the HER process might be the electrochemical desorption ($H^* + H_2O + e^- \rightarrow H_2 + OH^- + *$)[37]. Furthermore, the intrinsic activity of the synthesized samples is assessed through the exchange current density (j_0). Figure 3C and Supplementary Table 2 show that Pt_{QDs}@NiFe LDH has the highest j_0 of 4.325 $mA{\cdot}cm^{-2}$ compared to other control samples, indicating its excellent HER activity. Additionally, the $\Delta\eta/\Delta\log|j|$ within different ranges of current densities can be used to evaluate the mass transfer capability of electrocatalysts[42]. The variation of $\Delta\eta/\Delta\log|j|$ for Pt_{QDs}@NiFe LDH under different current densities is more gradual compared to Pt/C, especially at high current densities, indicating that Pt_{QDs}@NiFe LDH possesses superior HER activity [Figure 3D]. Additionally, the charge transfer rates of the prepared samples were evaluated using electrochemical impedance spectroscopy (EIS), and the equivalent circuit diagram is shown in Supplementary Figure 11. Figure 3E shows that Pt_{QDs}@NiFe LDH exhibits the smallest semicircle diameter of 1.62 Ω, lower than other samples, indicating its rapid charge transfer kinetics. Additionally, the electrocatalytic activity of Pt_{QDs}@NiFe LDH and other samples was further evaluated by testing the cyclic voltammetry (CV) in the non-Faraday region [Supplementary Figure 12]. Figure 3F shows that the double-layer capacitance (C_{dl}) of Pt_{QDs}@NiFe LDH is 55 $mF{\cdot}cm^{-2}$, significantly exceeding the values of other control samples. This reveals the exposure of numerous active sites in Pt_{QDs}@NiFe LDH, demonstrating its superior HER activity. Moreover, Figure 3G shows that Pt_{QDs}@NiFe LDH can operate stably for 55 h at 500 and 1000 $mA{\cdot}cm^{-2}$, indicating its excellent durability. Notably, Pt_{QDs}@NiFe LDH exhibits superior catalytic performance and rapid reaction kinetics at high current densities, surpassing most previously reported works [Figure 3H and Supplementary Table 3]. Furthermore, the catalytic activity of Pt_{QDs}@NiFe LDH at the temperature (65 ℃) of industrial electrolysis water was evaluated. As shown in Supplementary Figure 13, at 65 ℃, Pt_{QDs}@NiFe LDH does not exhibit significant decay and still demonstrates excellent HER activity and the potential for industrial applications. In addition, the acidic HER performance of prepared samples was tested in a three-electrode system in 0.5 M H_2SO_4 solution. As shown in Supplementary Figure 14A and 14B

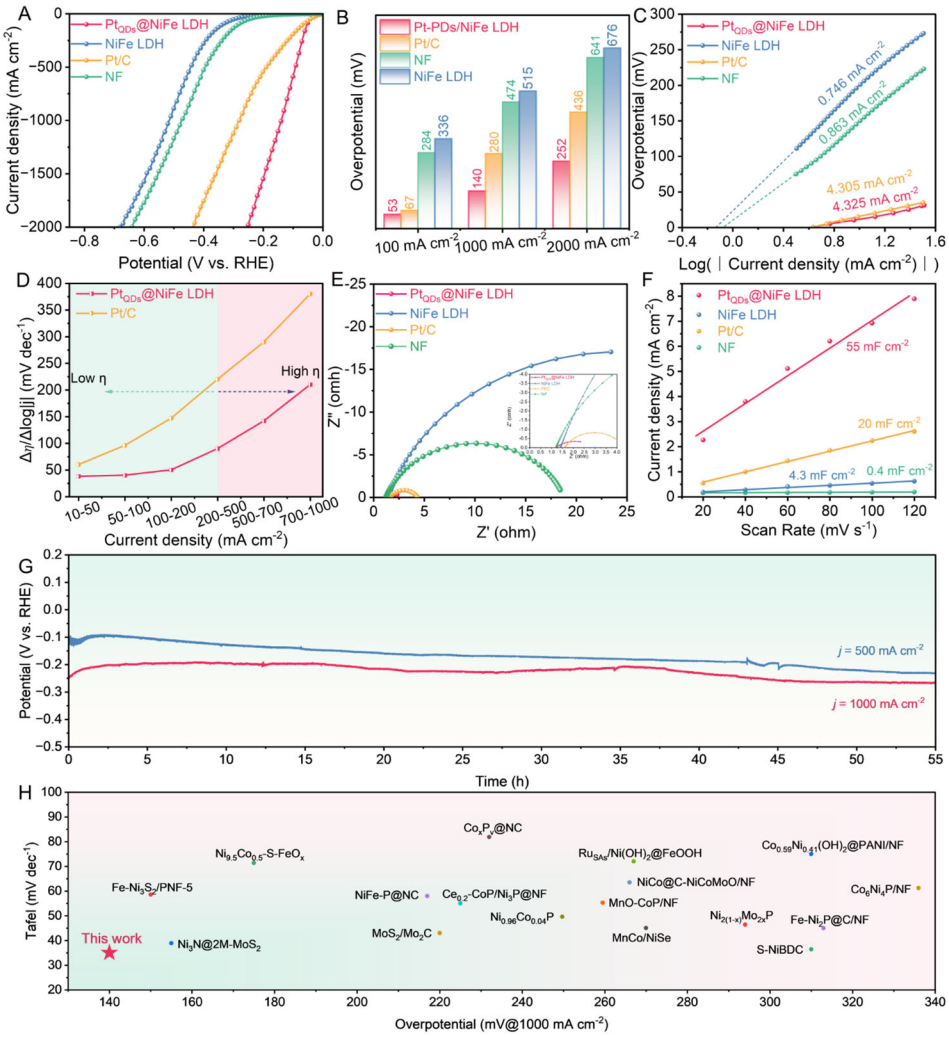

Figure 3. HER performance tests. (A) LSV curves. (B) The overpotentials at 100, 1000 and 2000 mA·cm^{-2}. (C) j_0 of Pt_{QDs}@NiFe LDH and other control samples are derived by Tafel plots. (D) Ratios of $\Delta\eta/\Delta\log|j|$ of Pt_{QDs}@NiFe LDH and Pt/C at different current density ranges. (E) Nyquist plots. (F) The C_{dl}. (G) Stability tests at 500 and 1000 mA·cm^{-2}. (H) Comparison of catalytic activity (overpotentials at 1000 mA·cm^{-2}) and HER kinetics (Tafel slopes) of Pt_{QDs}@NiFe LDH with other reported electrocatalysts.

, Pt_{QDs}@NiFe LDH exhibits superior HER catalytic activity under acidic conditions compared to other comparison samples. Specifically, Pt_{QDs}@NiFe LDH only requires overpotentials of 39, 59, and 85 mV to achieve 200, 500, and 800 mA·cm^{-2}, respectively. Furthermore, Pt_{QDs}@NiFe LDH can operate for 45 h at 200 mA·cm^{-2} with minimal performance degradation [Supplementary Figure 14C]. These results demonstrate that Pt_{QDs}@NiFe LDH possesses excellent HER performance and has potential for industrial application.

Overall water splitting performance

The overall water splitting (OWS) performance of electrocatalysts is an important criterion for evaluating their potential for industrial application. The OER is a critical component of OWS. Therefore, the OER activity of Pt_{QDs}@NiFe LDH-1, Pt_{QDs}@NiFe LDH, Pt_{QDs}@NiFe LDH-5 electrocatalysts, and a NiFe LDH precursor was tested. Figure 4A and 4B indicates that the NiFe LDH precursor exhibits superior OER performance compared to the samples loaded with Pt_{QDs}. Specifically, NiFe LDH requires low overpotentials of 318, 360, and 412 mV to realize 500, 1000, and 1500 mA·cm^{-2}, respectively, outperforming other compared samples. Furthermore, a two-electrode system was constructed using Pt_{QDs}@NiFe LDH with

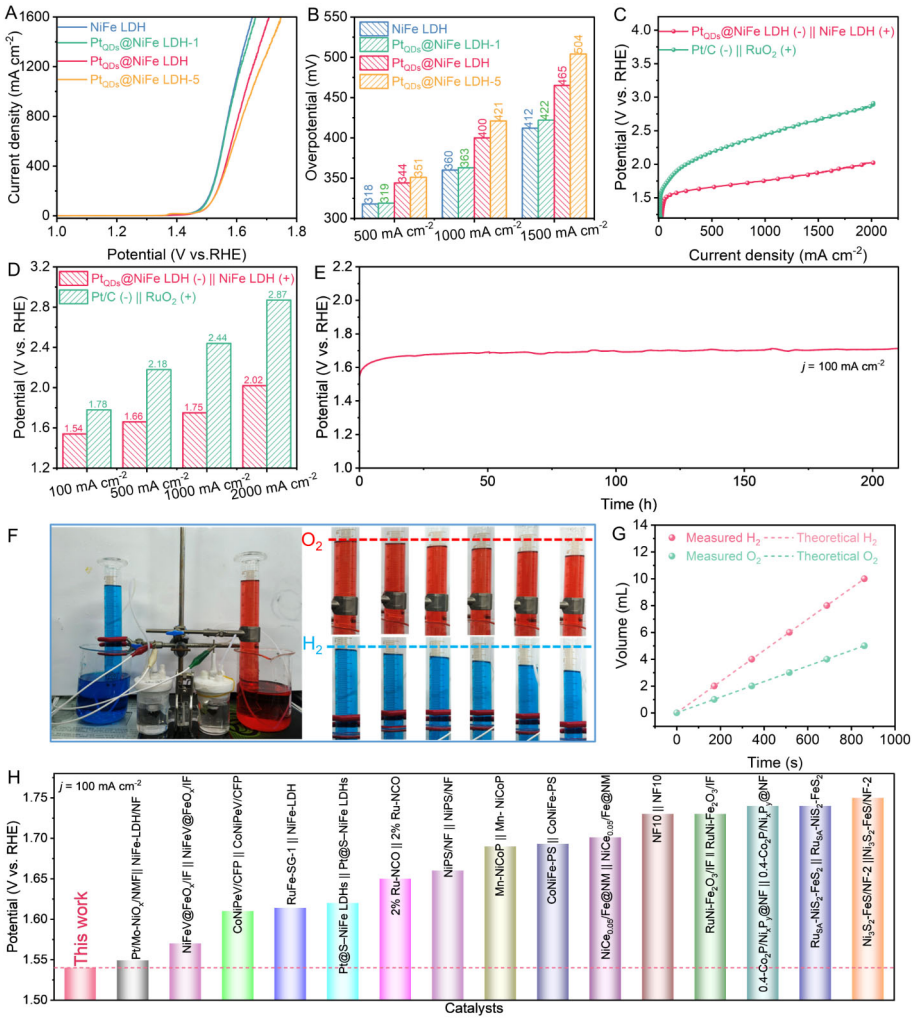

Figure 4. The OWS performance tests. (A) LSV curves of NiFe LDH, Pt_{QDs}@NiFe LDH-1, Pt_{QDs}@NiFe LDH, and Pt_{QDs}@NiFe LDH-5. (B) The overpotentials at 500, 1000 and 1500 mA·cm^{-2}. (C) LSV curves of Pt_{QDs}@NiFe LDH (-) || NiFe LDH (+) and Pt/C (-) || RuO_2. (D) The cell voltages at different current densities. (E) Stability tests. (F) Photographs of gas collection at different times. (G) Theoretical and measured gas production at different times. (H) Comparison of the driving voltage of Pt_{QDs}@NiFe LDH (-) || NiFe LDH (+) with other reported electrocatalysts.

excellent HER performance as the cathode electrode and NiFe LDH with superior OER activity as the anode electrode to evaluate the OWS performance [Pt_{QDs}@NiFe LDH (-) || NiFe LDH (+)]. For better comparison, another two-electrode system was assembled using Pt/C and RuO_2 as the cathode and anode electrodes, respectively, and named Pt/C (-) || RuO_2 (+). Figure 4C and 4D demonstrates that the Pt_{QDs}@NiFe LDH (-) || NiFe LDH (+) achieves superior water electrolysis performance at high current densities, significantly surpassing the Pt/C (-) || RuO_2 (+). Specifically, the Pt_{QDs}@NiFe LDH (-) || NiFe LDH (+) electrolyzer only requires 1.54, 1.75, and 2.02 V of the driving voltages to achieve 100, 1000, and 2000 mA·cm^{-2}, respectively, which is notably superior to the commercial Pt/C (-) || RuO_2 (+) electrolyzer, indicating that Pt_{QDs}@NiFe LDH (-) || NiFe LDH (+) has excellent OWS activity. Furthermore, the Pt_{QDs}@NiFe LDH (-) || NiFe LDH (+) electrolyzer can operate stably at 100 mA·cm^{-2} for 200 h, demonstrating outstanding durability [Figure 4E]. In addition, the Faraday efficiency (FE) of Pt_{QDs}@NiFe LDH (-) || NiFe LDH (+) was tested by the drainage method [Figure 4F]. Figure 4G shows that the measured ratio of H_2 to O_2 is 2 : 1, and the calculated FE is close to 100%, indicating its excellent catalytic activity. Additionally, the OWS performance

of the Pt_{QDs}@NiFe LDH (-) || NiFe LDH (+) electrolyzer outperforms the majority of catalysts reported in previous studies [Figure 4H and Supplementary Table 4]. These results suggest that Pt_{QDs}@NiFe LDH (-) || NiFe LDH (+) has significant potential for industrial applications.

CONCLUSIONS

In summary, a self-supported heterogeneous Pt_{QDs}@NiFe LDH electrocatalyst for water electrolysis at ampere-level current densities was successfully synthesized by coupling small and well-dispersed Pt_{QDs} with NiFe LDH nanosheets. The Pt_{QDs}@NiFe LDH exhibits attractive HER catalytic performance in an alkaline electrolyte, which achieves 500 and 1000 mA·cm^{-2} with low overpotentials of 92 and 140 mV, respectively, substantially lower than that of benchmark Pt/C (η_{500} = 190 mV, η_{1000} = 280 mV). In addition, Pt_{QDs}@NiFe LDH can operate stably at 500 and 1000 mA·cm^{-2} for 55 h, indicating its potential for scalable H_2 production. A series of materials characterizations indicate that there are strong electronic interactions between Pt_{QDs} and NiFe LDH in Pt_{QDs}@NiFe LDH, which optimizes the charge distribution and balances the adsorption/desorption of H intermediates on Pt_{QDs}@NiFe LDH, thereby enhancing the HER performance. Furthermore, when using the NiFe LDH precursor and the prepared Pt_{QDs}@NiFe LDH catalyst as the anode and cathode in an OWS system, which requires only 1.66 V and 2.02 V to reach 500 and 2000 mA·cm^{-2}, respectively, while maintaining robust stability for 200 hours. This study offers a reference for developing affordable and high-performance electrocatalysts for H_2 production under large current densities.

DECLARATIONS

Authors' contributions

Conceptualization, Investigation, Methodology, Data curation, Writing-Original draft: Wang B, Zhao X, Sun H
Conceptualization, Investigation, Software: Zhang M, Qiu G, Li D, Zhang J
Supervision, Project administration, Writing-review & editing: Sun H, Liu Q
Funding acquisition: Chen M, Zhang Y, Sun H, Liu Q
Validation, Software: Wu Y, Liu C, Yang H, Lu Q, Zhou T, Zhao J, Cui H, Liu F

Availability of data and materials

The raw data supporting the findings of this study are available within this Article and its Supplementary Information. Further data is available from the corresponding authors upon reasonable request.

Financial support and sponsorship

This work was funded by the National Key Research and Development Program of China (2022YFB3803600); the National Natural Science Foundation of China (22368050, 22378346), the Key Research and Development Program of Yunnan Province (202302AF080002); the Yunnan Basic Applied Research Project (202401AT070460, 202401AU070229); the Scientific Research Fund Project of Yunnan Education Department (2024J0014, 2024J0013); and the Open Project of Yunnan Precious Metals Laboratory Co.; Ltd (YPML-2023050259, YPML-2023050260). The authors thank the Shiyanjia Lab (www.shiyanjia.com), the Electron Microscopy Center, and the Advanced Analysis and Measurement Center of Yunnan University for the sample testing and computational services.

Conflicts of interest

Hao Cui and Feng Liu are affiliated with Yunnan Precious Metals Laboratory Co., Ltd.
The other authors declared that there are no conflicts of interest.

Ethical approval and consent to participate

Not applicable.

Consent for publication

Not applicable.

Copyright

REFERENCES

1. Mchugh, P. J.; Stergiou, A. D.; Symes, M. D. Decoupled electrochemical water splitting: from fundamentals to applications. *Adv. Energy. Mater.* **2020**, *10*, 2002453. DOI
2. He, X.; Han, X.; Zhou, X.; et al. Electronic modulation with Pt-incorporated NiFe layered double hydroxide for ultrastable overall water splitting at 1000 $mA{\cdot}cm^{-2}$. *Appl. Catal. B:. Environ.* **2023**, *331*, 122683. DOI
3. Lv, J.; Wang, L.; Li, R.; et al. Constructing a hetero-interface composed of oxygen vacancy-enriched Co_3O_4 and crystalline–amorphous NiFe-LDH for oxygen evolution reaction. *ACS. Catal.* **2021**, *11*, 14338-51. DOI
4. Zhai, P.; Xia, M.; Wu, Y.; et al. Engineering single-atomic ruthenium catalytic sites on defective nickel-iron layered double hydroxide for overall water splitting. *Nat. Commun.* **2021**, *12*, 4587. DOI PubMed PMC
5. Zhang, Y.; Zhao, M.; Wu, J.; et al. Construction of Pt Single-Atom and Cluster/FeOOH synergistic active sites for efficient electrocatalytic hydrogen evolution reaction. *ACS. Catal.* **2024**, *14*, 7867-76. DOI
6. Otto, F. E. L.; Skeie, R. B.; Fuglestvedt, J. S.; Berntsen, T.; Allen, M. R. Assigning historic responsibility for extreme weather events. *Nature. Clim. Change.* **2017**, *7*, 757-9. DOI
7. Vijayapradeep, S.; Kumar, R. S.; Karthikeyan, S.; Ramakrishnan, S.; Yoo, D. J. Constructing micro-nano rod-shaped iron-molybdenum oxide heterojunctions to enhance overall water electrolysis. *Mater. Today. Chem.* **2024**, *36*, 101934. DOI
8. Gao, X.; Chen, Y.; Wang, Y.; et al. Next-generation green hydrogen: progress and perspective from electricity, catalyst to electrolyte in electrocatalytic water splitting. *Nanomicro. Lett.* **2024**, *16*, 237. DOI PubMed PMC
9. Yu, B.; Tan, J.; Zhang, S. Uncertainties in the technological pathway towards low-carbon freight transport under carbon neutral target in China. *Appl. Energy.* **2024**, *365*, 123272. DOI
10. Lei, H.; Wan, Q.; Tan, S.; Wang, Z.; Mai, W. Pt-Quantum-Dot-Modified Sulfur-Doped NiFe layered double hydroxide for High-Current-Density alkaline water splitting at industrial temperature. *Adv. Mater.* **2023**, *35*, e2208209. DOI PubMed
11. Wang, L.; Xia, M.; Wang, H.; et al. Greening ammonia toward the solar ammonia refinery. *Joule* **2018**, *2*, 1055-74. DOI
12. Wu, Q.; Shen, C.; Rui, N.; Sun, K.; Liu, C. Experimental and theoretical studies of CO_2 hydrogenation to methanol on Ru/In2O3. *J. CO2. Util.* **2021**, *53*, 101720. DOI
13. Qiu, Z.; Du, T.; Yue, Q.; et al. A multi-parameters evaluation on exergy for hydrogen metallurgy. *Energy* **2023**, *281*, 128279. DOI
14. Zeng, Y.; Zhao, M.; Zeng, H.; et al. Recent progress in advanced catalysts for electrocatalytic hydrogenation of organics in aqueous conditions. *eScience* **2023**, *3*, 100156. DOI
15. Sun, S.; Wang, T.; Qian, K.; et al. Tailoring cation vacancies in Co, Ni phosphides for efficient overall water splitting. *Int. J. Hydrog. Energy.* **2022**, *47*, 39731-42. DOI
16. Xu, B.; Liang, J.; Sun, X.; Xiong, X. Designing electrocatalysts for seawater splitting: surface/interface engineering toward enhanced electrocatalytic performance. *Green. Chem.* **2023**, *25*, 3767-90. DOI
17. Gultom, N. S.; Abdullah, H.; Hsu, C.; Kuo, D. Activating nickel iron layer double hydroxide for alkaline hydrogen evolution reaction and overall water splitting by electrodepositing nickel hydroxide. *Chem. Eng. J.* **2021**, *419*, 129608. DOI
18. Guo, T.; Li, L.; Wang, Z. Recent development and future perspectives of amorphous transition metal-based electrocatalysts for oxygen evolution reaction. *Adv. Energy. Mater.* **2022**, *12*, 2200827. DOI
19. Li, X.; Zhang, H.; Hu, Q.; et al. Amorphous NiFe oxide-based nanoreactors for efficient electrocatalytic water oxidation. *Angew. Chem. Int. Ed. Engl.* **2023**, *62*, e202300478. DOI
20. Wei, J.; Zhou, M.; Long, A.; et al. Heterostructured electrocatalysts for hydrogen evolution reaction under alkaline conditions. *Nanomicro. Lett.* **2018**, *10*, 75. DOI PubMed PMC
21. Dao, H. T.; Hoa, V. H.; Sidra, S.; Mai, M.; Zharnikov, M.; Kim, D. H. Dual efficiency enhancement in overall water splitting with defect-rich and Ru atom-doped NiFe LDH nanosheets on $NiCo_2O_4$ nanowires. *Chem. Eng. J.* **2024**, *485*, 150054. DOI
22. Zhang, T.; Wu, M.; Yan, D.; et al. Engineering oxygen vacancy on NiO nanorod arrays for alkaline hydrogen evolution. *Nano. Energy.* **2018**, *43*, 103-9. DOI
23. Zhong, W.; Li, W.; Yang, C.; et al. Interfacial electron rearrangement: Ni activated $Ni(OH)_2$ for efficient hydrogen evolution. *J. Energy. Chem.* **2021**, *61*, 236-42. DOI
24. Lu, L.; Zhang, Y.; Chen, Z.; et al. Synergistic promotion of HER and OER by alloying ternary Zn-Co-Ni nanoparticles in N-doped carbon interfacial structures. *Chin. J. Catal.* **2022**, *43*, 1316-23. DOI
25. Chukwuneke, C. E.; Kawashima, K.; Li, H.; et al. Electrochemically engineered domain: nickel–hydroxide/nickel nitride composite for

alkaline HER electrocatalysis. *J. Mater. Chem. A.* **2024**, *12*, 1654-61. DOI
26. Huang, Z. F.; Song, J.; Li, K.; et al. Hollow cobalt-based bimetallic sulfide polyhedra for efficient all-ph-value electrochemical and photocatalytic hydrogen evolution. *J. Am. Chem. Soc.* **2016**, *138*, 1359-65. DOI
27. Bodhankar, P. M.; Sarawade, P. B.; Singh, G.; Vinu, A.; Dhawale, D. S. Recent advances in highly active nanostructured NiFe LDH catalyst for electrochemical water splitting. *J. Mater. Chem. A.* **2021**, *9*, 3180-208. DOI
28. Yao, H.; Le, F.; Jia, W.; et al. Dual electronic modulations on NiFeV Hydroxide@FeO_x boost electrochemical overall water splitting. *Small* **2023**, *19*, e2301294. DOI
29. Han, C.; Ji, Z.; Zhu, Y.; et al. Construction of Ni_3S_2 -Ni_xP_y/NF@NiFe LDH with heterogeneous interface to accelerate catalytic kinetics of overall water splitting. *Mater. Res. Lett.* **2022**, *10*, 762-70. DOI
30. Mohammed-ibrahim, J. A review on NiFe-based electrocatalysts for efficient alkaline oxygen evolution reaction. *J. Power. Sources.* **2020**, *448*, 227375. DOI
31. Huang, G.; Li, Y.; Chen, R.; et al. Electrochemically formed PtFeNi alloy nanoparticles on defective NiFe LDHs with charge transfer for efficient water splitting. *Chin. J. Catal.* **2022**, *43*, 1101-10. DOI
32. Chen, G.; Wang, T.; Zhang, J.; et al. Accelerated hydrogen evolution kinetics on nife-layered double hydroxide electrocatalysts by tailoring water dissociation active sites. *Adv. Mater.* **2018**, 30. DOI
33. Chen, Y.; Li, J.; Liu, T.; et al. Constructing robust NiFe LDHs–NiFe alloy gradient hybrid bifunctional catalyst for overall water splitting: one-step electrodeposition and surface reconstruction. *Rare. Met.* **2023**, *42*, 2272-83. DOI
34. Zhang, M.; Wang, B.; Sun, H.; et al. Electronic modulation of FeOOH coupled NiFe-LDH for highly efficient alkaline water oxidation at high current density. *Int. J. Hydrog. Energy.* **2024**, *60*, 1215-23. DOI
35. Tang, Y.; Liu, Q.; Dong, L.; Wu, H. B.; Yu, X. Activating the hydrogen evolution and overall water splitting performance of NiFe LDH by cation doping and plasma reduction. *Appl. Catal. B:. Environ.* **2020**, *266*, 118627. DOI
36. Yaseen, W.; Xie, M.; Yusuf, B. A.; et al. Anchoring $Ni(OH)_2$-CeOx heterostructure on FeOOH-modified nickel-mesh for efficient alkaline water-splitting performance with improved stability under quasi-industrial conditions. *Small* **2024**, *20*, e2403971. DOI
37. Wang, B.; Sun, H.; Chen, M.; et al. Ru single-atom regulated $Ni(OH)_2$ nanowires coupled with FeOOH to achieve highly efficient overall water splitting at industrial current density. *Chem. Eng. J.* **2024**, *479*, 147500. DOI
38. Yu, Z.; Sun, Q.; Zhang, L.; et al. Research progress of amorphous catalysts in the field of electrocatalysis. *Microstructures* **2024**, *4*, 2024022. DOI
39. Han, H. G.; Choi, J. W.; Son, M.; Kim, K. C. Unlocking power of neighboring vacancies in boosting hydrogen evolution reactions on two-dimensional $NiPS_3$ monolayer. *eScience* **2024**, *4*, 100204. DOI
40. Meng, L.; Zhang, L.; Liu, S.; Wang, F.; Wu, H. $Mo_{0.2}Ni_{0.8}N/CeO_2$ heterojunction as bifunctional electrocatalysts for overall urea-water electrolysis. *Int. J. Hydrog. Energy.* **2023**, *48*, 33383-92. DOI
41. Pan, Z.; Yaseen, M.; Kang, S. P.; Zhan, Y. Designing highly efficient 3D porous Ni-Fe sulfide nanosheets based catalyst for the overall water splitting through component regulation. *J. Colloid. Interface. Sci.* **2022**, *616*, 422-32. DOI PubMed
42. Sun, H.; Chen, H.; Humayun, M.; et al. Unlocking the catalytic potential of platinum single atoms for industry□level current density chlorine tolerance hydrogen generation. *Adv. Funct. Materials.* **2024**, *34*, 2408872. DOI
43. Zhu, Y.; Chen, Y.; Feng, Y.; Meng, X.; Xia, J.; Zhang, G. Constructing Ru-O-TM bridge in NiFe-LDH enables high current hydrazine-assisted H_2 production. *Adv. Mater.* **2024**, *36*, e2401694. DOI
44. Wang, X.; Tuo, Y.; Zhou, Y.; Wang, D.; Wang, S.; Zhang, J. Ta-doping triggered electronic structural engineering and strain effect in NiFe LDH for enhanced water oxidation. *Chem. Eng. J.* **2021**, *403*, 126297. DOI
45. Sun, H.; Li, L.; Humayun, M.; et al. Achieving highly efficient pH-universal hydrogen evolution by superhydrophilic amorphous/crystalline $Rh(OH)_3$/NiTe coaxial nanorod array electrode. *Appl. Catal. B:. Environ.* **2022**, *305*, 121088. DOI
46. Yang, Y.; Xie, Y.; Yu, Z.; et al. Self-supported NiFe-LDH@CoS_x nanosheet arrays grown on nickel foam as efficient bifunctional electrocatalysts for overall water splitting. *Chem. Eng. J.* **2021**, *419*, 129512. DOI
47. Chen, Z.; Li, X.; Zhao, J.; et al. Stabilizing pt single atoms through Pt-Se electron bridges on vacancy-enriched nickel selenide for efficient electrocatalytic hydrogen evolution. *Angew. Chem. Int. Ed. Engl.* **2023**, *62*, e202308686. DOI
48. Tan, L.; Wang, H.; Qi, C.; et al. Regulating Pt electronic properties on NiFe layered double hydroxide interface for highly efficient alkaline water splitting. *Appl. Catal. B:. Environ.* **2024**, *342*, 123352. DOI
49. Zhang, Q.; Xiao, W.; Fu, H. C.; et al. Unraveling the mechanism of self-repair of NiFe-based electrocatalysts by dynamic exchange of iron during the oxygen evolution reaction. *ACS. Catal.* **2023**, *13*, 14975-86. DOI
50. Li, X.; Liu, X.; Zhang, C.; et al. A corrosion-etching strategy for fabricating RuO_2 coupled with defective NiFeZn(OH)*x* for a highly efficient hydrogen evolution reaction. *J. Mater. Chem. A.* **2022**, *10*, 20453-63. DOI
51. Jiang, S.; Zhang, R.; Liu, H.; et al. Promoting formation of oxygen vacancies in two-dimensional cobalt-doped ceria nanosheets for efficient hydrogen evolution. *J. Am. Chem. Soc.* **2020**, *142*, 6461-6. DOI
52. Qin, Q.; Jang, H.; Jiang, X.; et al. Constructing interfacial oxygen vacancy and ruthenium Lewis acid-base pairs to boost the alkaline hydrogen evolution reaction kinetics. *Angew. Chem. Int. Ed. Engl.* **2024**, *63*, e202317622. DOI
53. An, C.; Wang, S.; Lin, L.; Ding, X.; Deng, Q.; Hu, N. Construction and ultrasonic inspection of the high-capacity Li-ion battery based on the MnO_2 decorated by Au nanoparticles anode. *Microstructures* **2024**, *4*, 2024003. DOI
54. Zhang, H.; Wu, L.; Feng, R.; et al. Oxygen vacancies unfold the catalytic potential of NiFe-Layered double hydroxides by promoting their electronic transport for oxygen evolution reaction. *ACS. Catal.* **2023**, *13*, 6000-12. DOI

55. Kim, D.; Resasco, J.; Yu, Y.; Asiri, A. M.; Yang, P. Synergistic geometric and electronic effects for electrochemical reduction of carbon dioxide using gold-copper bimetallic nanoparticles. *Nat. Commun.* **2014**, *5*, 4948. DOI PubMed
56. Liu, X.; Wang, R.; Chen, Y.; et al. Inhibitor-regulated corrosion strategy towards synthesizing cauliflower-like amorphous RuFe-hydroxides as advanced hydrogen evolution reaction catalysts. *Int. J. Hydrog. Energy.* **2023**, *48*, 9333-43. DOI